

MINIMIZING ANGLE ERROR IN 2D MAGNETIC SENSORS BY NONORTHOGONALITY CORRECTION

By Allegro MicroSystems

INTRODUCTION

Magnetic sensors can be used for rotation detection. For this, usually a small magnet is attached to a shaft (or any other rotational axis). Thus, when the shaft rotates, the magnetic sensor detects the change of the magnetic field orientation. Such magnetic sensors are also called two-dimensional (2D) magnetic sensors.

The main component of Allegro 2D magnetic sensors are based on arrays of magnetic tunnel junction (MTJ) cells (see Figure 1). Each MTJ cell is mainly composed of: 1) a pinned layer (PL), where the magnetization of such layer is fixed; 2) a sense layer (SL), where its magnetization can easily be oriented along the direction of the applied magnetic field; and 3) a tunnel barrier between both PL and SL.

The resistance, R , of each MTJ cell is dependent on the relative orientation, θ , between PL magnetization and SL magnetization due to the tunneling magnetoresistance (TMR) effect:

Equation 1:

$$R(\theta) = \frac{1}{G(\theta)} = \frac{1}{G_0 + \Delta G \times \cos\theta}$$

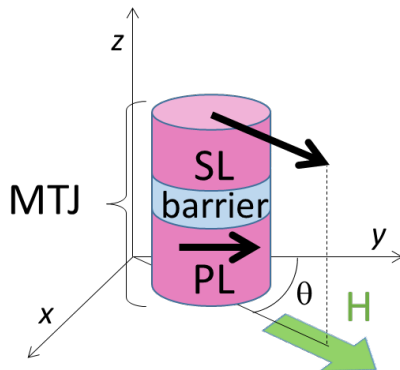


Figure 1: Effect of External Magnetic Field, H , on MTJ Cell

where G is the conductivity, ΔG is the change of conductivity due to the TMR effect, and G_0 is the average conductivity between parallel and antiparallel configurations of the MTJ structure.

Thus, by changing the orientation of the applied magnetic field, a variation of the output voltage is obtained.

A Wheatstone bridge architecture (see Figure 2) enables an output voltage, V_{OUT} , that is proportional to a sinusoidal signal with respect to θ to be obtained. For this, each branch of the Wheatstone bridge consists of an array of MTJ dots connected in series and/or parallel. The orientation of the PL (arrows in Figure 2) is similar for diagonal branches (R_1 and R_4 or R_2 and R_3 in Figure 2) and opposite for those branches constituting a half bridge (R_1 and R_2 or R_3 and R_4 in Figure 2). Considering this:

Equation 2:

$$\frac{V_{OUT}}{V_{DD}} = \left(\frac{R_2(\theta)}{R_1(\theta) + R_2(\theta)} - \frac{R_4(\theta)}{R_3(\theta) + R_4(\theta)} \right),$$

where V_{DD} is the applied voltage.

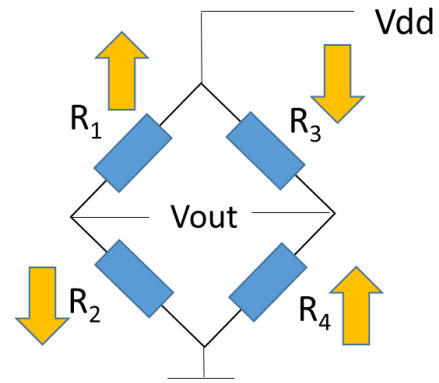


Figure 2: Schematic of a Wheatstone bridge architecture with 4 MTJ branches. Arrows show the orientation of the PL for each MTJ branch.

Therefore, if all branches have similar resistances, and considering Equation 1, V_{OUT} can be written as:

Equation 3:

$$\frac{V_{OUT}}{V_{DD}} = \left(\frac{TMR}{TMR + 2} \right) \times \cos\theta$$

However, to ensure an unambiguous determination of θ , 2D sensors are usually based on two Wheatstone bridges where the orientation of the PLs are mutually orthogonal. By this configuration, two voltage outputs, V_{SIN} and V_{COS} , are generated by the 2D sensor, where V_{COS} follows a cosine (COS) signal and V_{SIN} follows a sine (SIN) signal (see Figure 3). Thus, the measured angle, θ_{meas} , is determined by the arc tangent of the ratio between both signals:

Equation 4:

$$\theta_{meas} = \arctan\left(\frac{V_{SIN}}{V_{COS}}\right),$$

and angular error (AE) is the parameter that determines the accuracy of the measured angle θ_{meas} :

Equation 5:

$$AE = \theta_{meas} - \theta.$$

Several factors can lead, however, to a significant AE. One of the issues that is addressed in this application note is the parameter dependence of AE, as well as different correction approaches that can be considered to mitigate their impact on AE.

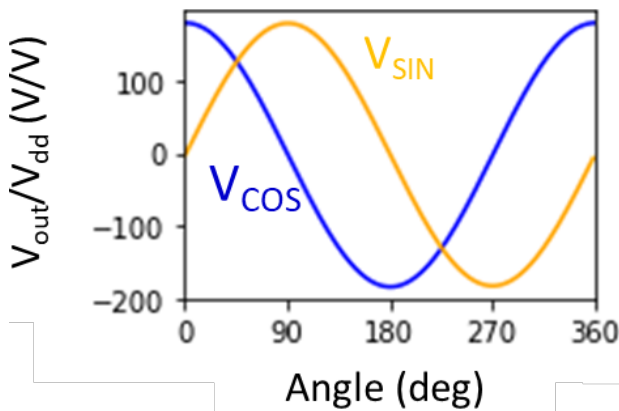


Figure 3: Typical angular dependence of the output voltage of a 2D magnetic sensor with two Wheatstone bridges, one orthogonally oriented with respect to the other.

PARAMETER DEPENDENCE OF AE

The output voltage of a 2D magnetic sensor with two Wheatstone bridges can generally be written as:

Equation 6:

$$V_{COS} = [A_{COS} \times \cos(\theta + \alpha_{COS}) + C_{COS}] \quad (a)$$

$$V_{SIN} = [A_{SIN} \times \sin(\theta + \alpha_{SIN}) + C_{SIN}] \quad (b)$$

where A_{COS} , A_{SIN} are the amplitude, C_{COS} , C_{SIN} are the offset and α_{COS} , α_{SIN} are the phase shift of both COS and SIN bridges. Note that both amplitudes and offsets are now normalized parameters with respect to the applied voltage V_{DD} ; therefore, V_{COS} and V_{SIN} can be expressed in mV/V.

Ideally, if both bridges present no offset ($C_{COS} = C_{SIN} = 0$) and no phase shift ($\alpha_{COS} = \alpha_{SIN} = 0$), and their amplitudes are the same ($A_{COS} = A_{SIN}$), $AE = 0$. Any situation different from this leads to an $AE \neq 0$.

The impact on AE for such parameters is summarized in Figure 4, Figure 5, and Figure 6. The behavior of AE increase is shown with: amplitude changes (ΔA_{COS} and ΔA_{SIN}) in Figure 4; offset changes in Figure 5; and phase-shift changes in Figure 6.

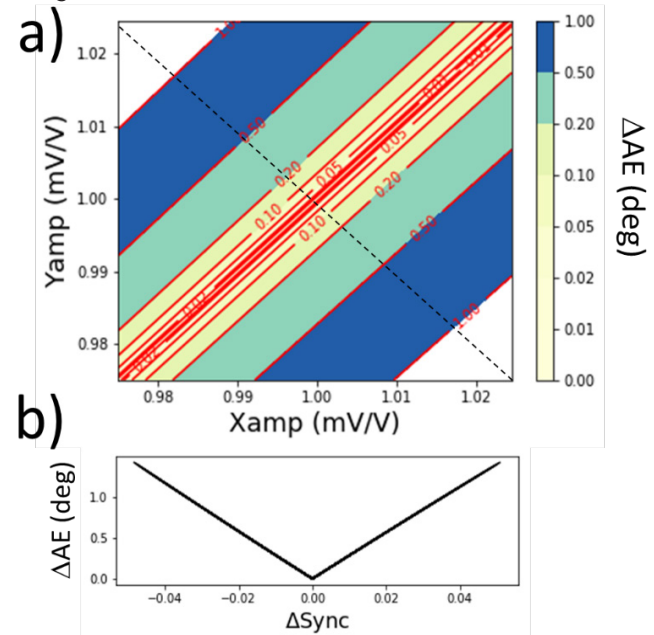


Figure 4: a) Increase of AE due to amplitude increase on both bridges, where ΔX_{amp} and ΔY_{amp} are the variation ratio of both amplitude voltages., and the dashed lines show increase of Sync direction; b) ΔAE vs. $\Delta Sync$.

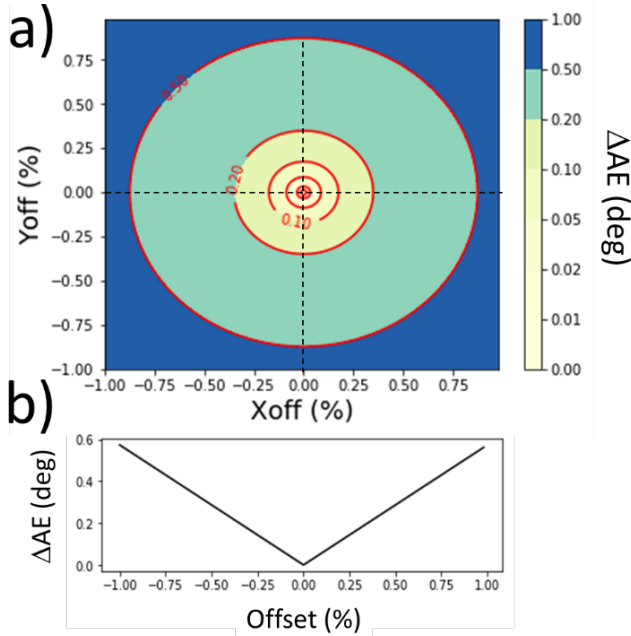


Figure 5: a) Increase of AE due to offset increase on both bridges, where ΔX_{off} and ΔY_{off} are the variation ratio of both offset voltages; b) ΔAE vs. $\Delta Total$ Offset.

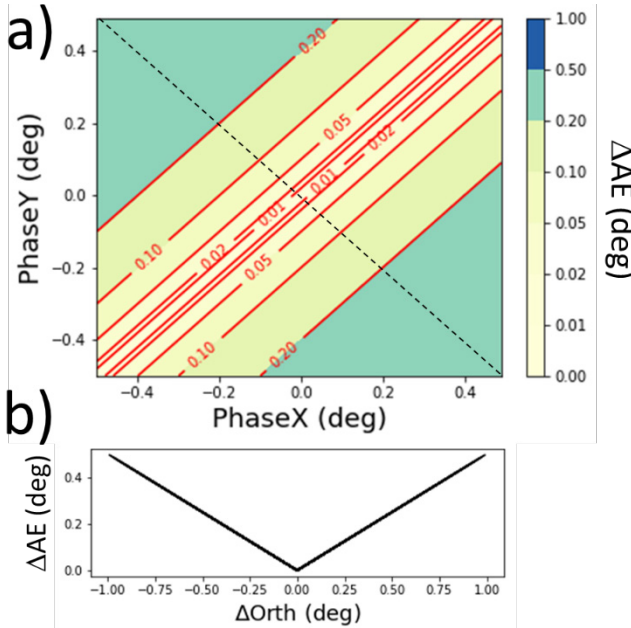


Figure 6: a) Increase of AE due to phase-shift increase on both bridges, where the dashed lines show increase of nonorthogonality; b) ΔAE vs. $\Delta Orth$.

In all three figures, normalized output voltages (V_{COS}/A_{COS} and V_{SIN}/A_{SIN}) are considered; therefore, Equation 6a and Equation 6b become:

Equation 7:

$$v_{COS} = \cos(\theta + \alpha_{COS}) + (C_{COS}/A_{COS}) \quad (a)$$

$$v_{SIN} = \sin(\theta + \alpha_{SIN}) + (C_{SIN}/A_{SIN}) \quad (b)$$

Initial conditions are with no offset ($C_{COS} = C_{SIN} = 0$) or phase shift ($\alpha_{COS} = \alpha_{SIN} = 0$) for an ideal 2D sensor. Changes in amplitudes and offsets can therefore be expressed in percentage (%) with respect to their initial amplitudes, A_{COS} and A_{SIN} . Dashed lines in Figure 5a, Figure 6a, and Figure 7a show the direction of variation of synchronism ($Sync = A_{COS}/A_{SIN}$), total offset ($C = \sqrt{C_{COS}^2 + C_{SIN}^2}$), and nonorthogonality (Non-Orth) between both bridges. As can be observed from these figures, these are the real parameters that determine AE.

The variation of AE vs. Sync, total offset, and Non-Orth are plotted in Figure 4b, Figure 5b, and Figure 6b, respectively. In all three cases, ΔAE is linear with respect to their variation (For a summary of such variations, see Table 1).

Note that the harmonic contributions to the AE are not the same for all three parameters (see Table 1). The angular dependence of AE for all three cases are shown in Figure 7: a) $Sync \neq 1$ (AE_{Sync}); b) $Offset \neq 0$ (AE_{Off}); and c) nonorthogonality $\neq 0$ (AE_{Orth}). As can be observed, mismatch amplitude (Figure 8a) and phase shift (Figure 7c) induce each of them an AE with a periodicity of π (second harmonic) while offset contributions induce an AE with a periodicity of 2π (first harmonic). Each contribution to the AE could therefore be expressed as:

Equation 8:

$$AE_{Sync} = AE_{Sync}^0 \times \sin(2\theta) \quad (a)$$

$$AE_{Off} = -AE_{Off}^0 \times \sin(\theta - \varphi) \quad (b)$$

$$AE_{Orth} = AE_{Orth}^0 \times [1 + \cos(2\theta)] \quad (c)$$

where AE_{Sync}^0 , AE_{Off}^0 and AE_{Orth}^0 are the slopes of Figure 4b, Figure 5b, and Figure 6b, respectively, the values of which are shown in Table 1 and $\varphi = \arctan(C_{SIN}/C_{COS})$.

Table 1: ΔAE Ratio for Each Parameter Increase and Its Harmonic Contribution to AE

Parameter Increase	ΔAE (°)	Harmonic Contribution
Sync	0.29°/0.01	2nd
Total Offset	0.6°/%	1st
Orth	0.5°/°	2nd

These equations show that no possible cancelation of AE can be obtained by the combination of all three contributions. However, it also implies that the total AE induced by a combination of three such contributions is always smaller than the addition of each individual contribution. The total AE obtained when combining all three contributions (Figure 7a, Figure 7b, and Figure 7c) is shown in Figure 7d to be $\sim 1.16^\circ$, which is smaller than $0.57^\circ + 0.57^\circ + 0.50^\circ = 1.64^\circ$. Note that Figure 7d can be obtained either by calculating the total AE from Equation 6a and Equation 6b or by adding Equation 8a, Equation 8b, and Equation 8c.

It is clear, therefore, that mismatched amplitudes (or synchronism) and offsets of V_{OUT} —as well as nonorthogonality between both bridges—can have a big impact on AE. The following proposed correction methods enable rectification of such contributions to improve accuracy on angle determination.

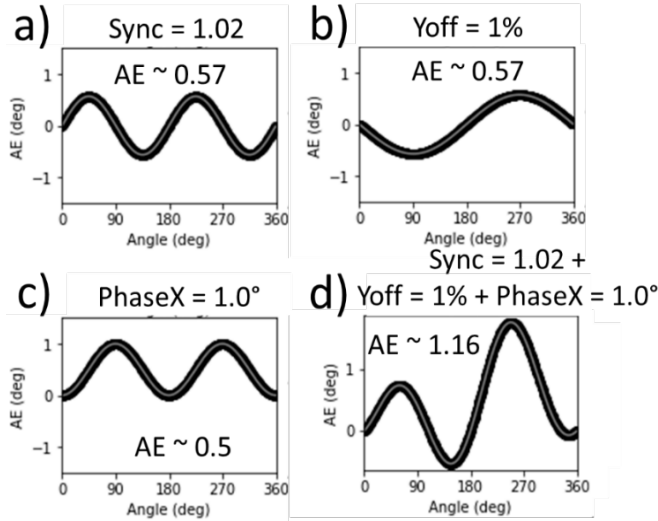


Figure 7: Angular dependence of AE for a) $Sync = 1.02$, $C_{COS} = C_{SIN} = 0$, and $\alpha_{COS} = \alpha_{SIN} = 0$; b) $Sync = 1.0$, $C_{SIN}/A_{SIN} = 1\%$, $C_{COS} = 0$, and $\alpha_{COS} = \alpha_{SIN} = 0$; c) $Sync = 1.0$, $C_{COS} = C_{SIN} = 0$, $\alpha_{SIN} = 0$, and $\alpha_{COS} = 1.0^\circ$

Method 1: AENorm

This method (also called “normalization correction”) consists on the subtraction of the offset and normalization of the output voltage of each bridge. By this, V_{COS}^{norm} and V_{SIN}^{norm} are obtained:

Equation 9:

$$V_{COS}^{norm} = (V_{COS} - C_{COS})/A_{COS} \quad (a)$$

$$V_{SIN}^{norm} = (V_{SIN} - C_{SIN})/A_{SIN} \quad (b)$$

By considering Equation 6a and Equation 6b, this means:

Equation 10:

$$V_{COS}^{norm} = \cos(\theta + \alpha_{COS}) \quad (a)$$

$$V_{SIN}^{norm} = \sin(\theta + \alpha_{SIN}) \quad (b)$$

Thus, the measured angle is determined by the arc tangent ratio between V_{SIN}^{norm} and V_{COS}^{norm} :

Equation 11:

$$\theta_{meas}^{norm} = \arctan\left(\frac{V_{SIN}^{norm}}{V_{COS}^{norm}}\right),$$

and the normalized angular error (AENorm) would be:

Equation 12:

$$AENorm = \theta_{meas}^{norm} - \theta.$$

This correction method only requires a first calibration procedure consisting of performing a unique rotational loop measurement. Then, by determining the maximum and minimum output voltages for each bridge, A_{COS}^0 , A_{SIN}^0 , C_{COS}^0 , and C_{SIN}^0 can be determined:

Equation 13:

$$A_{COS}^0 = (V_{COS}^{max} - V_{COS}^{min})/2 \quad (a)$$

$$C_{COS}^0 = (V_{COS}^{max} + V_{COS}^{min})/2 \quad (b)$$

$$A_{SIN}^0 = (V_{SIN}^{max} - V_{SIN}^{min})/2 \quad (c)$$

$$C_{SIN}^0 = (V_{SIN}^{max} + V_{SIN}^{min})/2 \quad (d)$$

Such A_{COS}^0 , A_{SIN}^0 , C_{COS}^0 , and C_{SIN}^0 parameters can then be used as parameter corrections of all measured data (V_{COS} and V_{SIN}), such that:

Equation 14:

$$V_{COS}^{norm} = (V_{COS} - C_{COS}^0)/A_{COS}^0 \quad (a)$$

$$V_{SIN}^{norm} = (V_{SIN} - C_{SIN}^0)/A_{SIN}^0 \quad (b)$$

and the measured angle is determined by Equation 11.

Important improvements to AE can be obtained when considering the normalization of output voltages as observed in Figure 8. In this case, similar contributions of Sync, offset and phase shift, as observed in Figure 7d are considered. By this correction method, reduction of AE from $\sim 1.16^\circ$ (black curve) to $\sim 0.5^\circ$ (red curve) is obtained.

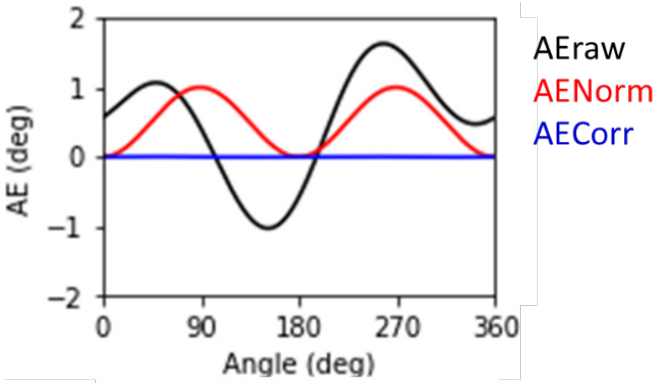


Figure 8: Angular dependence of AE for 2D sensor with $\text{Sync} = 1.02$, $C_{SIN} / A_{SIN} = 1\%$ and $\alpha_{COS} = 1.0^\circ$. AErAw (black curve) refers to the AE derived without any correction method. AENorm (red curve) refers to the AE derived from normalization correction. AECorr (blue curve) refers to the AE derived from nonorthogonality correction method.

Method 2: AECorr

Large reduction of AE can be obtained by normalization calibration (AENorm). However, possible contribution on AE from nonorthogonality can still be present as observed in Figure 8 (see red curve). Indeed, in such a case, a nonorthogonality of 1.0° leads to an AENorm of $\sim 0.5^\circ$.

To remove such an effect, Equation 10a and Equation 10b need to be expanded as:

Equation 15:

$$V_{COS}^{norm} = \cos\theta \times \cos\alpha_{COS} - \sin\theta \times \sin\alpha_{COS} \quad (a)$$

$$V_{SIN}^{norm} = \sin\theta \times \cos\alpha_{SIN} + \cos\theta \times \sin\alpha_{SIN} \quad (b)$$

Then, considering small orthogonality deviations (i.e., small phase shifts of α_{COS} and $\alpha_{SIN} \rightarrow 0^\circ$), the following is obtained:

Equation 16:

$$V_{COS}^{norm} \sim \cos\theta - \alpha_{COS} \times \sin\theta \quad (a)$$

$$V_{SIN}^{norm} \sim \sin\theta + \alpha_{SIN} \times \cos\theta \quad (b)$$

This, can be expressed in the following matrix form:

Equation 17:

$$\begin{bmatrix} V_{SIN}^{norm} \\ V_{COS}^{norm} \end{bmatrix} = \begin{bmatrix} 1 & \alpha_{SIN} \\ -\alpha_{COS} & 1 \end{bmatrix} \cdot \begin{bmatrix} \sin\theta \\ \cos\theta \end{bmatrix}$$

Then, by inverting this system of matrix equations and keeping only linear terms of α_{COS} and α_{SIN} , the following results:

Equation 18:

$$\begin{bmatrix} \sin\theta \\ \cos\theta \end{bmatrix} = \begin{bmatrix} 1 & -\alpha_{SIN} \\ \alpha_{COS} & 1 \end{bmatrix} \cdot \begin{bmatrix} V_{SIN}^{norm} \\ V_{COS}^{norm} \end{bmatrix}$$

Which is equivalent to:

Equation 19:

$$\sin\theta \sim V_{SIN}^{norm} - \alpha_{SIN} \times V_{COS}^{norm} \quad (a)$$

$$\cos\theta \sim \alpha_{COS} \times V_{SIN}^{norm} + V_{COS}^{norm} \quad (b)$$

Thus, the measured angle is determined by:

Equation 20:

$$\theta_{meas}^{corr} = \arctan\left(\frac{V_{SIN}^{norm} - \alpha_{SIN} \times V_{COS}^{norm}}{\alpha_{COS} \times V_{SIN}^{norm} + V_{COS}^{norm}}\right),$$

and the corrected angular error (AECorr) is described as:

Equation 21:

$$AECorr = \theta_{meas}^{corr} - \theta$$

This correction method (also called “nonorthogonality correction”) requires, like the normalization correction method, a first calibration procedure consisting of performing a unique rotational-loop measurement. After this measurement, and in order to derive all required parameters (A_{COS}^0 , A_{SIN}^0 , C_{COS}^0 , and C_{SIN}^0 , α_{COS}^0 and α_{SIN}^0) both V_{COS} and V_{SIN} data need to be fitted following Equation 6a and Equation 6b. Then, considering such parameters as parameter corrections for all next measured data (V_{COS} and V_{SIN}), the measured angle can therefore be determined by Equation 9a, Equation 9b, and Equation 20.

Complete reduction of AE can be achieved by this correction method. Figure 8 shows the performance of “nonorthogonality correction” to reduce AE $\sim 0^\circ$ (blue curve) in comparison to previous “normalization correction” (red curve).

As a matter of fact, Equation 20 enables AE corrections for nonorthogonality values up to 2° . AECorr derived from Equation 20 for a large range of nonorthogonality values exhibiting almost a quadratic dependence is shown in Figure 9a. Thus, for nonorthogonality $< 1^\circ$, an AECorr as low as 0.001° could be obtained, which is close to the maximum AE resolution such sensors usually hold. However, in the case that unusually large nonorthogonality values ($> 5^\circ$) are present, a more-general expression must be considered.

Indeed, Equation 15a and Equation 15b can be expressed in the following matrix form:

Equation 22:

$$\begin{bmatrix} V_{SIN}^{norm} \\ V_{COS}^{norm} \end{bmatrix} = \begin{bmatrix} \cos\alpha_{SIN} & \sin\alpha_{SIN} \\ -\sin\alpha_{COS} & \cos\alpha_{COS} \end{bmatrix} \cdot \begin{bmatrix} \sin\theta \\ \cos\theta \end{bmatrix}$$

Then, by inverting this system of matrix equations, the following is obtained:

Equation 23:

$$\begin{bmatrix} \sin\theta \\ \cos\theta \end{bmatrix} = \frac{1}{K} \begin{bmatrix} \cos\alpha_{COS} & -\sin\alpha_{SIN} \\ \sin\alpha_{COS} & \cos\alpha_{SIN} \end{bmatrix} \cdot \begin{bmatrix} V_{SIN}^{norm} \\ V_{COS}^{norm} \end{bmatrix}$$

where $K = \cos(\alpha_{SIN} - \alpha_{COS})$.

Thus, the measured angle is determined by:

Equation 24:

$$\theta_{meas}^{corr} = \arctan\left(\frac{\cos\alpha_{COS} \times V_{SIN}^{norm} - \sin\alpha_{SIN} \times V_{COS}^{norm}}{\sin\alpha_{COS} \times V_{SIN}^{norm} + \cos\alpha_{SIN} \times V_{COS}^{norm}}\right)$$

Figure 9b shows that such generalized nonorthogonal correction method enables a reduced AE of $\sim 0^\circ$ (see green curve), even for a nonorthogonality of $\sim 30^\circ$.

Therefore, in general, nonorthogonality correction enables achievement of higher angle accuracy than normalized correction, without adding much complexity to the one-step calibration operation.

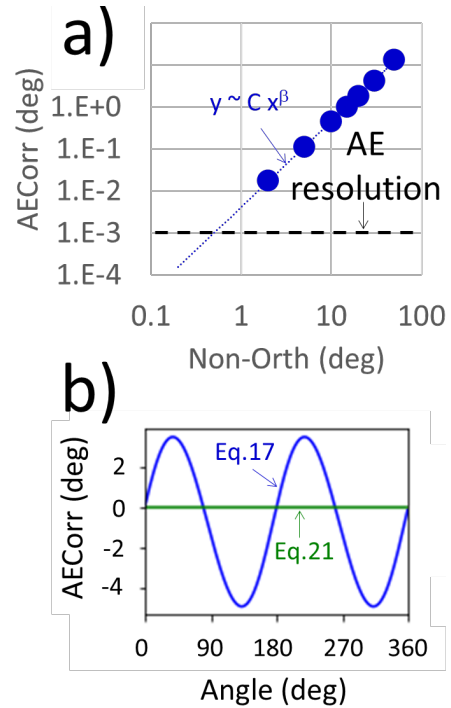


Figure 9: a) AECorr (determined by Equation 20) vs. nonorthogonality. Black dashed lines indicate the usual AE resolution in a 2D magnetic sensor. $C \sim 0.0041$ and $\beta \sim 2.04$; b) angular dependence of AECorr with nonorthogonality of 30° when determining AECorr by Equation 20 (blue curve) or by Equation 24 (green curve).

STABILITY OF CORRECTION

After such corrections, all 2D magnetic sensors are able to guarantee an $AENom < AENorm_0$ (where $AENorm_0$ is the maximum AE after normalization correction) or an $AECorr < AECorr_0$ (where $AECorr_0$ is the maximum AE after nonorthogonality correction).

Moreover, the parameters derived from the one-step calibration procedure in both correction methods ($A_{COS}^0, A_{SIN}^0, C_{COS}^0$, and C_{SIN}^0 for normalization correction; or $A_{COS}^0, A_{SIN}^0, C_{COS}^0$, and $C_{SIN}^0, \alpha_{COS}^0$ and α_{SIN}^0 for nonorthogonality correction) are used during the entire lifetime of the sensor. This implies that such correction methods need to be stable for all working conditions; in other words, $AENorm$ (or $AECorr$) must be stable for a certain temperature and magnetic field range.

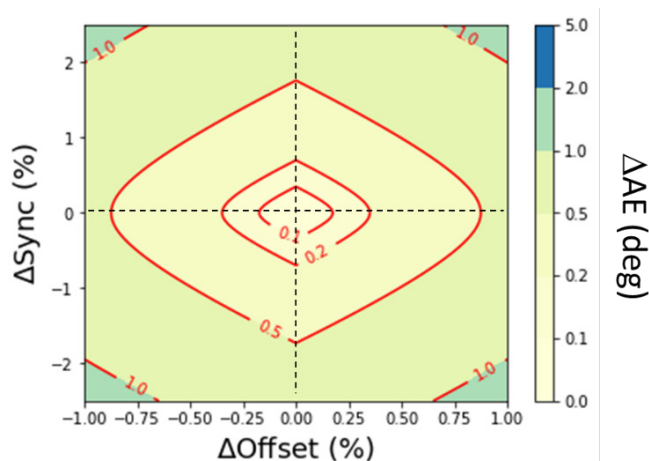


Figure 10: ΔAE map vs. $\Delta Sync$ and $\Delta Offset$. Here, nonorthogonality was considered (α_{COS} and $\alpha_{COS} = 0$).

To guarantee this, it is important to ensure a minimum variation of synchronism, offset, and orthogonality under such working conditions. A map of ΔAE vs. variation of $\Delta Sync$ and $\Delta Offset$ is shown in Figure 10. The contour lines of constant ΔAE follow a diamond-like shape. This map enables, therefore, the determination of all possible variations of Sync and Offset that a 2D magnetic sensor could experience in order to guarantee an increase of AE below a certain level. Thus, for instance, to ensure that, after one-step calibration, the sensors have a maximum increase of $\Delta AENorm < 0.1^\circ$ with temperature, it would be necessary, according to Figure 10, that

$\Delta Sync < 0.3\%$ and $\Delta Offset < 0.6\%$ (see stars on Figure 10).

Note, that a similar conclusion could also be obtained from Table 1, which is therefore very useful to quickly determine the maximum variation of Sync, total offset, and orthogonality for a certain increase of AE (ΔAE).

Similar analysis can also be performed for a nonorthogonality correction method that would enable determination of the maxo,i, variation of all three parameters to ensure a stable $AECorr$.

To conclude, stability of synchronism, offset, and orthogonality are therefore crucial to ensure that calibration methods such as a one-step calibration process would be used during the whole lifetime of the sensor

SUMMARY

Amplitude mismatch (synchronism), offset, and nonorthogonality between both Wheatstone bridges impact the accuracy of the measured angle in 2D sensors. Several correction methods to minimize the AE induced by such parameters have been presented here.

The first method relies on normalization of measured voltages, enabling removal of synchronism and offset contributions. This simple technique requires a one-time calibration operation and basic calculation computation. After correction parameters are derived, they are used for rectification of all subsequent measurements. This method, however, does not correct nonorthogonality contributions on AE.

The second method relies on complete correction (amplitude mismatch, offset, and nonorthogonality) of measured voltages by a fitting procedure. This technique also requires a one-time calibration operation with only one additional calculation step with respect to normalization correction. After correction parameters are derived, subsequent measurements are rectified by using such parameters.

By such corrections, the maximum AE of the 2D magnetic sensor can be substantially reduced, improving the accuracy of the measured angle.

Both correction methods rely on the stability of synchronism, offset, and nonorthogonality with respect other parameters like temperature and magnetic field.

Revision History

Number	Date	Description	Responsibility
1	November 14, 2023	Document rebrand and minor editorial corrections	J. Henry

Copyright 2023, Allegro MicroSystems.

The information contained in this document does not constitute any representation, warranty, assurance, guaranty, or inducement by Allegro to the customer with respect to the subject matter of this document. The information being provided does not guarantee that a process based on this information will be reliable, or that Allegro has explored all of the possible failure modes. It is the customer's responsibility to do sufficient qualification testing of the final product to ensure that it is reliable and meets all design requirements.

Copies of this document are considered uncontrolled documents.